Dynamics and computed torque control stability of an under-actuated tendon-driven manipulator

Nicolas J.S. Testard, Christine Chevallereau, Philippe Wenger

Dynamics and computed torque control stability of an under-actuated tendon-driven manipulator

Nicolas J.S. Testard, Christine Chevallereau, and Philippe Wenger

Nantes Université, Centrale Nantes, CNRS, LS2N, 44300 Nantes

Abstract. Tendon-driven manipulators have interesting properties such as reduced inertia and a better behavior w.r.t. physical interactions through the possible modulation of their stiffness. A 2-tendon-driven manipulator inspired by the bird neck is studied in this paper. The manipulator is remotely actuated with two tendons and only one output variable can be controlled. When applying a computed torque control, we observe that the control of one joint is stable but the control of the other joint is unstable. The goal of this paper is to provide a physical interpretation of this behavior. Instability is explained through the study of the dynamics in open-loop. Experiments are conducted that confirm the aforementioned behavior.

Keywords: Under-actuated, Tendon-driven, Dynamics, Control

1 Introduction

New manipulators can be developed through bio-inspiration. Examples of robots inspired by animals are elephant trunk arms [1], octopus' robots [2] or bird-neck manipulators [3]. Birds use their neck like humans use their arms. The bird neck architecture makes it possible to perform fast and complicated motions. Unlike the elephant trunk, the bird neck has a spine. Musculoskeletal systems can be modeled with cables and springs that play the role of tendons and ligaments and rigid bars that play the role of bones [4]. Actuation is done by varying the length of the tendons. Bird neck inspired robots can be modelled as a stack of anti-parallelogram joints (*X-joints*) that represents the motion between two vertebrae and each joint is actuated through two tendons [5]. These robots are thus fully-actuated and each joints can be controlled independently. However, it has been observed in [6] that the use of under-actuated robots can increase the size of the feasible workspace. Moreover, under-actuation allows the robot to shape around obstacles [7]. A planar, under-actuated robot with 6 joints and 4 tendons was presented in [8]. Because of the under-actuation, however, its control is challenging as dynamic control laws can be unstable, [8] proposes an unusual control law in the operational space without proof of its stability. To understand the difficulties of the control of such robots, this article studies the dynamics of the simplest under-actuated manipulator made of X-joints. The simplest manipulator is made of two X-joints and is actuated by two tendons. The results are then extended to manipulators with more X-joints. We apply

the computed torque control that linearizes the dynamic equation [9] to under-actuated systems [10]. This control has been applied on other under-actuated manipulators like the parallel robot of [11] or the cable-driven parallel robot of [12]. As observed in [13] for under-actuated cable-driven parallel robots, it will be seen that the computed torque control can be unstable. This instability can be explained by the fact that an under-actuated system can be a non minimum phase system [14] [15] depending on the studied control degree of freedom [16] [17]. However, the source of instability of under-actuated manipulators control has not been investigated further.

The purpose of this article is to explain the instability of the computed torque control through the dynamic properties of the manipulator. The dynamics of the system in open loop and the stability of the computed torque control for the control of each joint is presented through experiments.

2 Presentation of the manipulator

The simplest manipulator is composed of 2 X-joints as shown in Fig. 1. Each X-joint is composed of 4 bars, where b (resp. L) is the length of the top and base bars (resp. of the diagonal bars). The top bar of the first joint is the bottom bar of the second joint. The configuration of each joint i is defined by the angle α_i between the bottom bar and the top bar.

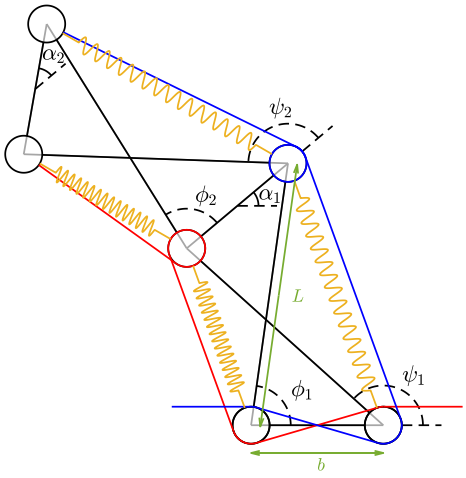

Fig. 1: Under-actuated tendon-driven manipulator

The resulting manipulator is actuated by 2 tendons, shown in blue and red in 1. These tendons are pulled by remote motors through winches (not shown in the figure). One tendon pulls the two joints on one side while the other tendon pulls on the opposite side. Pulleys are used to route the tendons while reducing

friction. We have added springs in parallel to the tendons in order that the robot has a stable equilibrium configuration at rest. All springs are identical, so that the equilibrium configuration at rest is $[\alpha_1, \alpha_2] = [0, 0]$.

3 Manipulator dynamics

The manipulator dynamics can be expressed by [3]:

$$\mathbf{M}_\alpha(\boldsymbol{\alpha})\ddot{\boldsymbol{\alpha}} + \boldsymbol{c}(\boldsymbol{\alpha}, \dot{\boldsymbol{\alpha}}) + \boldsymbol{g}(\boldsymbol{\alpha}) = \mathbf{Z}(\boldsymbol{\alpha})\boldsymbol{f} - \boldsymbol{f}_r(\boldsymbol{\alpha}, \dot{\boldsymbol{\alpha}}) \tag{1}$$

where:

- $\boldsymbol{\alpha} = [\alpha_1, \alpha_2]^\top$
- $\mathbf{M}_\alpha(\boldsymbol{\alpha})$ is the mass matrix of the manipulator,
- $\boldsymbol{g}(\boldsymbol{\alpha})$ is the effect linked to the potential energy of the springs,
- $\boldsymbol{c}(\boldsymbol{\alpha}, \dot{\boldsymbol{\alpha}})$ are the Coriolis and centrifugal effects,
- $\mathbf{Z}(\boldsymbol{\alpha}) = -\frac{\partial \boldsymbol{l}}{\partial \boldsymbol{\alpha}}^\top$, where $\boldsymbol{l} = [l_L, l_R]^\top$ are the tendons length, is the matrix that links the tension in the tendons to the torques they produced around the joint,
- $\boldsymbol{f} = [f_L, f_R]^\top$ is the vector tendon tensions,
- $\boldsymbol{f}_r(\boldsymbol{\alpha}, \dot{\boldsymbol{\alpha}})$ is a viscous friction in the joints of the form $f_v \left(2 \left(\frac{\partial \boldsymbol{\phi}}{\partial \boldsymbol{\alpha}} \right)^2 + 2 \left(\frac{\partial \boldsymbol{\psi}}{\partial \boldsymbol{\alpha}} \right)^2 \right) \dot{\boldsymbol{\alpha}}$ where $\boldsymbol{\phi} = [\phi_1, \phi_2]^\top$ and $\boldsymbol{\psi} = [\psi_1, \psi_2]^\top$ (see Fig. 1)

Gravity is neglected in this paper.

It is apparent from the expression of $\mathbf{Z}(\boldsymbol{\alpha})$ that the left (resp. right) tendon applies positive (resp. negative) torques on both joints since the derivatives of its length is negative (resp. positive). To visualize the dynamics behaviour of the robot, a simulation is made. Starting from a stable equilibrium configuration $\boldsymbol{\alpha} = [0, 0]^\top$ associated to $\boldsymbol{f} = [10, 10]^\top$N, a step of tension in the first tendons is applied, and the force became $\boldsymbol{f} = [20, 10]^\top$N.

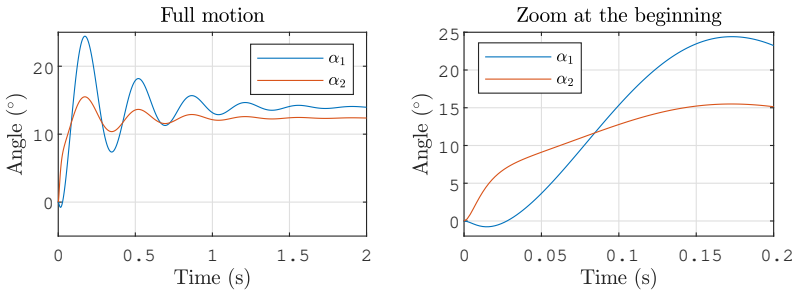

Fig. 2: Open loop simulation

Figure 2 shows the joint evolution. The data are those of our prototype: $b = 0.05$ m, $L = 0.1$ m; mass of the top (resp. diagonal) bars is 162 g (resp. 26 g); spring stiffness is 600 N/m. f_v is taken as 0.02 N.m/(rad/s). This friction dissipates the energy and allows the mechanism to reach a steady position after a perturbation.

The robot starts from a stable equilibrium configuration $\boldsymbol{\alpha} = [0, 0]^\top$ and moves towards a stable configuration $\boldsymbol{\alpha} = [14.0°, 12.4°]^\top$ after some oscillations (see Fig. 2, left). At the beginning, however, we observe that α_1 starts in the opposite direction before converging towards the desired position (see Fig. 2, right).

To study this initial opposite acceleration, we define:

$$\mathbf{B}(\boldsymbol{\alpha}) = \mathbf{M}_\alpha^{-1}(\boldsymbol{\alpha})\mathbf{Z}(\boldsymbol{\alpha}) \tag{2}$$

that links the tension in the tendons to the acceleration they produce on the joint.

$$\mathbf{M}_\alpha = \begin{pmatrix} M_{11} & M_{12} \\ M_{12} & M_{22} \end{pmatrix}, \quad \mathbf{Z} = \begin{pmatrix} Z_{1L} & Z_{1R} \\ Z_{2L} & Z_{2R} \end{pmatrix}, \quad \mathbf{B} = \begin{pmatrix} B_{1L} & B_{1R} \\ B_{2L} & B_{2R} \end{pmatrix}, \tag{3}$$

The computation of any static configuration with positive tension such that $\boldsymbol{g}(\boldsymbol{\alpha}) = \mathbf{Z}(\boldsymbol{\alpha})\boldsymbol{f}$ (Eq. (1)) leads to $\alpha_1 \approx \alpha_2$ (note that $\alpha_1 = \alpha_2$ only if the radius of the pulleys was neglected). In these configurations, thus, we can define $Z_L = Z_{1L} \approx Z_{2L} \geq 0$ and $Z_R = Z_{1R} \approx Z_{2R} \leq 0$. The computation of the components of matrix $\mathbf{B}$ with the above approximation is (for X equal to L or R):

$$\begin{aligned} B_{1X} &\approx (M_{22} - M_{12})Z_X / det(\mathbf{M}_\alpha) \\ B_{2X} &\approx (M_{11} - M_{12})Z_X / det(\mathbf{M}_\alpha) \end{aligned} \tag{4}$$

In the static equilibrium configurations, we also observe that $M_{11} \geq M_{12} \geq M_{22}$. Thus, B_{1L} and B_{2R} are positive while B_{1R} and B_{2L} are negative. The tendons produce an acceleration in the same direction as the torque for the second joint, but the first joint will have an acceleration in the opposite direction.

This unusual phenomenon of the opposite initial acceleration is therefore due to the particular actuation with tendons that pulls the joints on one side, as well as to the inertia properties of the manipulator. It is a classical property of non minimal phase systems.

4 Manipulator control

4.1 Computed torque control

The manipulator is controlled through two tendons. Since tendons can pull only, one degree of freedom is used to ensure that the tendons remain always in tension. Thus, only one degree of freedom can be controlled in the manipulator. This

degree of freedom q can be one of the joints or the end-effector orientation $\gamma = \alpha_1 + \alpha_2$ for example. The computed torque control based on the dynamics of the manipulator is used to control it.

The equation (1) can be rewritten as:

$$\ddot{\boldsymbol{\alpha}} + \mathbf{M}_{\alpha}^{-1}(\boldsymbol{\alpha})\left(\boldsymbol{c}(\boldsymbol{\alpha}, \dot{\boldsymbol{\alpha}}) + \boldsymbol{g}(\boldsymbol{\alpha}) + \boldsymbol{f}_r(\boldsymbol{\alpha}, \dot{\boldsymbol{\alpha}})\right) = \mathbf{B}(\boldsymbol{\alpha})\boldsymbol{f} \tag{5}$$

The dynamics of the controlled variable $q = \alpha_1$ (resp. $q = \alpha_2$, $q = \gamma$) is obtained by projecting on the matrix $\mathbf{J} = [1, 0]$ (resp. $\mathbf{J} = [0, 1]$, $\mathbf{J} = [1, 1]$):

$$\ddot{q} + \mathbf{J}\mathbf{M}_{\alpha}^{-1}(\boldsymbol{\alpha})\left(\boldsymbol{c}(\boldsymbol{\alpha}, \dot{\boldsymbol{\alpha}}) + \boldsymbol{g}(\boldsymbol{\alpha}) + \boldsymbol{f}_r(\boldsymbol{\alpha}, \dot{\boldsymbol{\alpha}})\right) = \mathbf{J}\mathbf{B}(\boldsymbol{\alpha})\boldsymbol{f} \tag{6}$$

Once the dynamics of one joint is expressed, a control of the the joint acceleration is performed. For a desired motion of one joint q^d, the close-loop acceleration is chosen as:

$$w = \ddot{q}^d + k_p(q^d - q) + k_d(\dot{q}^d - \dot{q}) + k_i \int (q^d - q)dt \tag{7}$$

where k_p, k_d and k_i are the constants of a PID correction.

Finally, the tendon tension providing the expected accelerations is:

$$\boldsymbol{f} = (\mathbf{J}\mathbf{B}(\boldsymbol{\alpha}))^{+} w_c + \lambda \mathbf{N}_{\mathbf{JB}} \tag{8}$$

where

$$w_c = w + \mathbf{J}\mathbf{M}_{\alpha}^{-1}(\boldsymbol{\alpha})\left(\boldsymbol{g}(\boldsymbol{\alpha}) + \boldsymbol{c}(\boldsymbol{\alpha}, \dot{\boldsymbol{\alpha}}) + \boldsymbol{f}_r(\boldsymbol{\alpha}, \dot{\boldsymbol{\alpha}})\right) \tag{9}$$

and $\mathbf{N}_{\mathbf{JB}}$ is the null space vector of $\mathbf{JB}$ and λ is scalar chosen such that the tension in the tendons are minimal and greater than a desired minimal tension.

The scheme of the control law is presented Fig. 3.

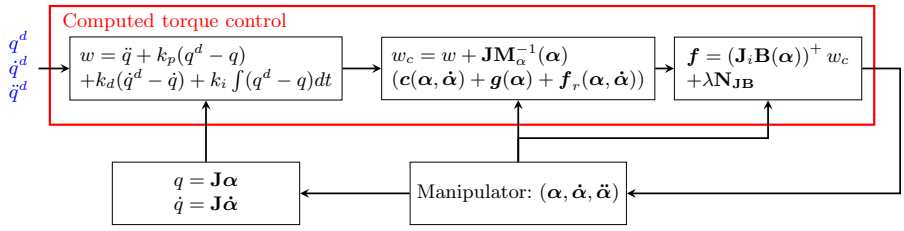

Fig. 3: Computed torque control scheme

4.2 Control stability

We have observed in simulation that, for any manipulator configuration and any desired trajectory, the control of α_2 is stable while the control of α_1 is unstable with the computed torque control.

It turns out that the dynamics of α_1 actuated by the tendons is a non-minimum phase system. To observe it, the transfer function of the linearized dynamic system can be studied. The linearization around a static point $\boldsymbol{\alpha}_0$ with tension $\boldsymbol{f}_0$ of Eq. (1) gives:

$$\mathbf{M}\ddot{\boldsymbol{\alpha}}_* + \mathbf{D}\dot{\boldsymbol{\alpha}}_* + \mathbf{K}\boldsymbol{\alpha}_* = \mathbf{Z}(\boldsymbol{\alpha}_0)\boldsymbol{f}_* \tag{10}$$

where $\boldsymbol{\alpha}_* = \boldsymbol{\alpha} - \boldsymbol{\alpha}_0$, $\boldsymbol{f}_* = \boldsymbol{f} - \boldsymbol{f}_0$, $\mathbf{M} = \mathbf{M}_\alpha(\boldsymbol{\alpha}_0)$, $\mathbf{D} = \dfrac{\partial \boldsymbol{f}_r}{\partial \dot{\boldsymbol{\alpha}}}(\boldsymbol{\alpha}_0, 0)$ and $\mathbf{K} = \dfrac{\partial(\boldsymbol{g} - \mathbf{Z}\boldsymbol{f})}{\partial \boldsymbol{\alpha}}(\boldsymbol{\alpha}_0)$.

This equation can be expressed in the Laplace domain [18]:

$$(\mathbf{M}s^2 + \mathbf{D}s + \mathbf{K})\boldsymbol{A}_* = \mathbf{Z}(\boldsymbol{\alpha}_0)\boldsymbol{F}_* \tag{11}$$

where s is the Laplace variable, $\boldsymbol{A}_*$ (resp. $\boldsymbol{F}_*$) is associated to $\boldsymbol{\alpha}_*$ (resp. $\boldsymbol{f}_*$) in the Laplace domain. The transfer function between the Laplace variable $\boldsymbol{Q}_*$ associated to q and $\boldsymbol{F}_*$ is therefore $\mathbf{H}(s) = \mathbf{J}(\mathbf{M}s^2 + \mathbf{D}s + \mathbf{K})^{-1}\mathbf{Z}(\boldsymbol{\alpha}_0)$. Each term of $\mathbf{H}(s)$, which describes the evolution of q in open-loop for a tension $\boldsymbol{f}$, is a fraction of polynomials. The roots of the numerator are the zeros of the transfer function while the roots of the denominator are the poles.

For any robot configuration associated to positive tendon tensions and friction, we have found that the zeros of the transfer functions between α_1 and $\boldsymbol{f}$ have a positive real part. Instead, the zeros of the transfer functions between α_2 or γ and $\boldsymbol{f}$ have all a negative real part.

When the computed torque control is applied on the system, these zeros become poles. Thus, the control of α_1 has poles with a positive real part in the transfer function of the control law, making the control unstable. In contrast, the control of α_2 and γ is stable since all the poles have a negative real part.

5 Experiments

This phenomenon is similar to results in continuum robotics like a flexible bar actuated by a rotational joint: in [19], for example, there is an uncontrolled degree of freedom which is due to the flexibility of the bar. However, the instability met in our system is not cause by flexibility. Indeed, we still meet the same instability when the springs are removed.

Experiments have been carried out on the prototype of Fig. 4. Encoders measure the angle ψ_1 for the first joint and the angle ϕ_2 of the second joint such that the angles $\boldsymbol{\alpha}$ can be computed. The tendons are wounded around winches.

A first open-loop experiment is presented in Fig. 5. A step of tension from $\boldsymbol{f} = [10, 10]^\top$N to $\boldsymbol{f} = [20, 10]^\top$N is imposed in the tendons.

At the beginning, α_1 goes in the opposite direction as in the simulation of Fig. 2. The rest of the motion is similar to the simulation Fig. 2. The oscillations are different because the friction has not been well identified and is different from the one used in simulation (non-linear dry friction was not taken into account).

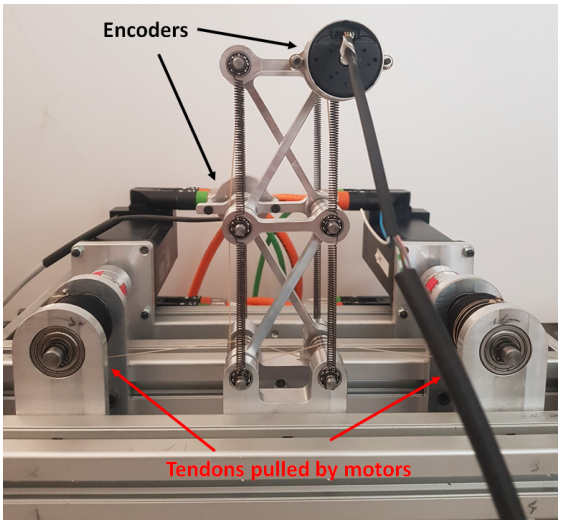

Fig. 4: Prototype

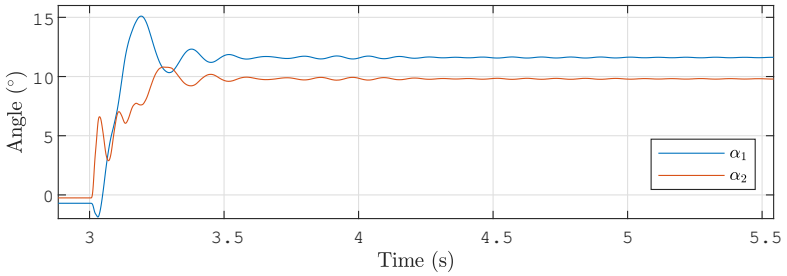

Fig. 5: Joint angles evolution of the open loop experiments

Figures 6 and 7 show a control of α_2 and α_1 with the computed torque control where a minimal tension of 10 N is imposed. We observe in Fig. 6 that there is a good tracking of α_2 trajectory while α_1 is left uncontrolled.

In Fig. 7, instead, the control of α_1 is unstable. Indeed, α_1 first is moving toward the desired value and then diverges in the opposite direction. Saturation in the tendons tension were applied to limit the motion and to avoid tendon rupture. As explained in Section 4.2, the opposite acceleration in α_1 at the beginning is the cause of this divergence. Indeed, a positive acceleration is desired in this motion and the use of matrix $\mathbf{B}$ by the computed torque control produces tension in the tendons associated to a negative torque (the right tendon is pulling, generating an initial positive acceleration of α_1). The corresponding static equilibrium for a negative torque being a negative angle, the manipulator goes in the opposite direction. The term $\alpha_1^d - \alpha_1$ in the PID correction of w_1

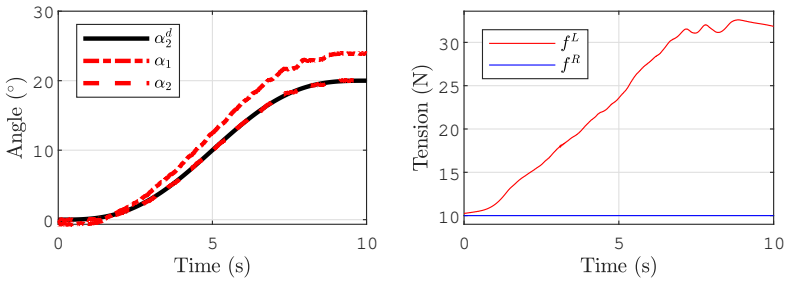

Fig. 6: Joint angles and tension evolution for the control of α_2

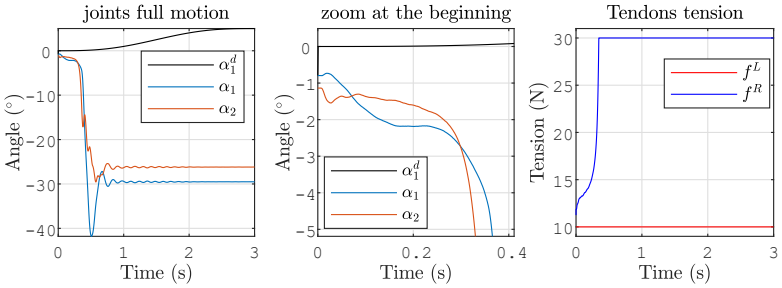

Fig. 7: Joint angles and tension evolution for the control of α_1

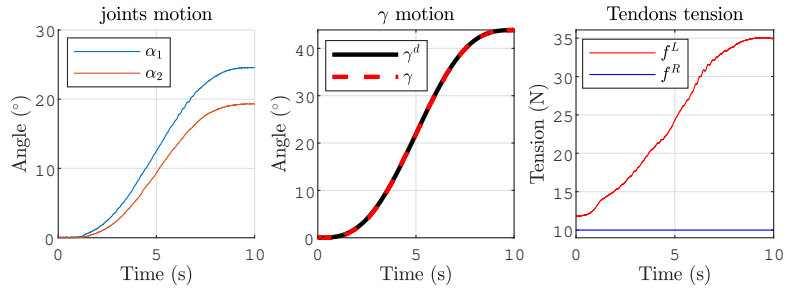

Fig. 8: Joint angles, γ and tension evolution for the control of γ

increases the positive desired acceleration, which makes the robot diverge until tendon tensions reach their limits.

Figure 8 shows the control of γ, which turns out to be stable. It can be explained by the fact that for any static configuration of the manipulator, $|B_{2X}| > |B_{1X}|$. Thus, the second joint has a greater absolute acceleration than the first joint and the acceleration of γ is in the same direction as the produced torque.

6 Generalization to several joints

The same study can be conducted on manipulators with a higher number of joints and still actuated through two tendons pulling on both sides of the joints. For manipulators with 3, 4, 5 and 6 joints, we have analyzed the stability like in Section 4.2. It turns out that only the control of the last joint is stable while the control all the other joints is unstable. The control of γ is also stable, which would indicate that the part of the last joint is preponderant as compared to the others in the control stability, or that there is a compensation between the unstable joints. These results have been confirmed by simulation but are not illustrated here for lack of space.

7 Conclusion

An under-actuated manipulator with two degrees of freedom and its dynamics have been presented. Between two static configurations after a perturbation in the tendon tensions, the two joints have opposite accelerations. The first joint goes first in the opposite direction instead of directly converging to its static position like the second joint. Because of this, the control of the first joint angle is unstable with the computed torque control. Indeed, the tensions producing an acceleration of α_1 in one direction correspond to a static position of α_1 in the opposite direction. This phenomenon is similar to the one observed in some continuum robots. The difference with these robots is that this phenomenon is due to the actuation and the inertia properties of the manipulator and not to flexibilities. More generally, for manipulators with two tendons and several joints, only the last joint can be stabilized with the computed torque control scheme.

The stability of the computed torque control can be studied for other controlled variables such as the position of the end-effector. The dynamic study and application of the computed torque control can also be conducted on under-actuated manipulators with more tendons.

References

1. M. Hannan and I. Walker, "Analysis and initial experiments for a novel elephant's trunk robot," in Proceedings. 2000 IEEE/RSJ International Conference on Intelligent Robots and Systems (IROS 2000) (Cat. No.00CH37113), vol. 1, pp. 330–337 vol.1, 2000.
2. C. Laschi, M. Cianchetti, B. Mazzolai, L. Margheri, M. Follador, and P. Dario, "Soft robot arm inspired by the octopus," Advanced Robotics, vol. 26, no. 7, pp. 709–727, 2012.
3. B. Fasquelle, P. Khanna, C. Chevallereau, D. Chablat, D. Creusot, S. Jolivet, P. Lemoine, and P. Wenger, "Identification and Control of a 3-X Cable-Driven Manipulator Inspired From the Bird's Neck," Journal of Mechanisms and Robotics, vol. 14, Feb. 2022. Publisher: American Society of Mechanical Engineers.
4. R. E. Skelton and M. C. De Oliveira, Tensegrity systems, vol. 1. Springer, 2009.

5. M. Furet, M. Lettl, and P. Wenger, "Kinematic analysis of planar tensegrity 2-X manipulators," in 16th International Symposium on Advances in Robot Kinematics, (Bologne, Italy), July 2018.
6. N. J. S. Testard, C. Chevallereau, and P. Wenger, "Comparison Analysis of Tendon-Driven Manipulators Based on Their Wrench Feasible Workspace," in Cable-Driven Parallel Robots (S. Caro, A. Pott, and T. Bruckmann, eds.), Mechanisms and Machine Science, (Cham), pp. 121–133, Springer Nature Switzerland, 2023.
7. D. L. Bakker, D. Matsuura, Y. Takeda, and J. L. Herder, "Design of an environmentally interactive continuum manipulator," in Proc. 14th World Congress in Mechanism and Machine Science, IFToMM, 2015.
8. N. J. S. Testard, C. Chevallereau, and P. Wenger, "Control in the operational space of a redundant and under-actuated tensegrity robot," in 25ème Congrès Français de Mécanique, (Nantes, France), Aug. 2022.
9. C. An, C. Atkeson, J. Griffiths, and J. Hollerbach, "Experimental evaluation of feedforward and computed torque control," in 1987 IEEE International Conference on Robotics and Automation Proceedings, vol. 4, pp. 165–168, Mar. 1987.
10. M. Reyhanoglu, A. van der Schaft, N. Mcclamroch, and I. Kolmanovsky, "Dynamics and control of a class of underactuated mechanical systems," IEEE Transactions on Automatic Control, vol. 44, pp. 1663–1671, Sept. 1999.
11. G. Jeanneau, V. Bégoc, and S. Briot, "Experimental Safety Analysis of R-Min, an underactuated parallel Robot," Journal of Mechanisms and Robotics, vol. 15, pp. 1–21, Jan. 2023.
12. A. A. Kumar, J.-F. Antoine, and G. Abba, "Input-Output Feedback Linearization for the Control of a 4 Cable-Driven Parallel Robot," IFAC-PapersOnLine, vol. 52, pp. 707–712, Jan. 2019.
13. A. A. Kumar, J.-F. Antoine, and G. Abba, "Control of an Underactuated 4 Cable-Driven Parallel Robot using Modified Input-Output Feedback Linearization," IFAC-PapersOnLine, vol. 53, pp. 8777–8782, Jan. 2020.
14. C. I. Byrnes and A. Isidori, "Local stabilization of minimum-phase nonlinear systems," Systems & Control Letters, vol. 11, pp. 9–17, July 1988.
15. D. CHEN and B. PADEN, "Stable inversion of nonlinear non-minimum phase systems," International Journal of Control, vol. 64, pp. 81–97, May 1996. Publisher: Taylor & Francis _eprint: https://doi.org/10.1080/00207179608921618.
16. E. G. Gilbert, "The decoupling of multivariable systems by state feedback," SIAM Journal on Control, vol. 7, no. 1, pp. 50–63, 1969.
17. A. Isidori, A. Krener, C. Gori-Giorgi, and S. Monaco, "Nonlinear decoupling via feedback: A differential geometric approach," IEEE Transactions on Automatic Control, vol. 26, pp. 331–345, Apr. 1981. Conference Name: IEEE Transactions on Automatic Control.
18. R. J. Beerends, H. G. ter Morsche, J. C. van den Berg, and E. M. van de Vrie, Fourier and Laplace Transforms. Cambridge: Cambridge University Press, 2003.
19. Y. Aoustin, C. Chevallereau, A. Glumineau, and C. Moog, "Experimental results for the end-effector control of a single flexible robotic arm," IEEE Transactions on Control Systems Technology, vol. 2, pp. 371–381, Dec. 1994. Conference Name: IEEE Transactions on Control Systems Technology.